High-resolution X-ray absorption spectroscopy as a probe of crystal-field and covalency effects in actinide compounds

Sergei Butorin, Kristina Kvashnina, Johan Vegelius, Daniel Meyer, David Shuh

High-resolution X-ray absorption spectroscopy as a probe of crystal-field and covalency effects in actinide compounds

Sergei M. Butorin[a,1], Kristina O. Kvashnina[b,c], Johan R. Vegelius[a], Daniel Meyer[d], and David K. Shuh[e]

[a]Molecular and Condensed Matter Physics, Department of Physics and Astronomy, Uppsala University, SE-751 20 Uppsala, Sweden; [b]The European Synchrotron, 38043 Grenoble, France; [c]Institute of Resource Ecology, Helmholtz-Zentrum Dresden-Rossendorf, 01314 Dresden, Germany; [d]Institut de Chimie Séparative de Marcoule, UMR 5257 Commissariat à l'Energie Atomique et aux Energie Alternative/CNRS/Université de Montpellier/Ecole Nationale Supérieure de Chimie de Montpellier, 30207 Bagnols-sur-Cèze, France; and [e]Chemical Sciences Division, Lawrence Berkeley National Laboratory, Berkeley, CA 94720

Edited by Zachary Fisk, University of California, Irvine, CA, and approved May 23, 2016 (received for review February 1, 2016)

Applying the high-energy resolution fluorescence-detection (HERFD) mode of X-ray absorption spectroscopy (XAS), we were able to probe, for the first time to our knowledge, the crystalline electric field (CEF) splittings of the 5*f* shell directly in the HERFD-XAS spectra of actinides. Using ThO_2 as an example, data measured at the Th 3*d* edge were interpreted within the framework of the Anderson impurity model. Because the charge-transfer satellites were also resolved in the HERFD-XAS spectra, the analysis of these satellites revealed that ThO_2 is not an ionic compound as previously believed. The Th 6*d* occupancy in the ground state was estimated to be twice that of the Th 5*f* states. We demonstrate that HERFD-XAS allows for characterization of the CEF interaction and degree of covalency in the ground state of actinide compounds as it is extensively done for 3*d* transition metal systems.

actinide compounds | crystal field | covalency

For strongly electron-correlated systems, X-ray absorption spectroscopy (XAS) is viewed as a technique capable of providing information on the ground-state character despite the presence of the core hole in the final state of the spectroscopic process. In the 3*d* transition metal compounds, XAS at the metal 2*p* edge is routinely used to probe the magnitude of the crystalline electric field (CEF) splittings in the 3*d* shell and the degree of the 3*d* hybridization in the ground state (1).

However, for the 5*f* shell of actinides, such a use of XAS is difficult. At the U 3*d* and 4*d* edges, where the transitions to the 5*f* states are probed, core-hole lifetime broadenings [full width at half maximum (FWHM)] are about 3.2 eV and 4.2 eV, respectively (2), whereas at the 5*d* edge, the broadening can be as large as 6.0 eV. Therefore, the conventional XAS spectra of actinide materials at the 3*d* and 4*d* edges often appear as single lines where splittings of the 5*f* states (e.g., due to the CEF interaction) are completely smeared out (3–8).

The CEF effects for actinides are usually characterized with the help of optical absorption (reviewed in ref. 9) and electron paramagnetic resonance (EPR) (10, 11) spectroscopies but that is often done on doped systems when the actinide ions in question are introduced into the lattice of a compound without 5*f* electrons. Another high-resolution technique that can provide information about the CEF splittings is inelastic neutron scattering (INS) (12, 13) but the spectra usually cover a very limited energy range. In both optical absorption and INS spectroscopies, the CEF strength and parameters are evaluated by fitting the calculated energy levels of the CEF Hamiltonian to the energies of the measured lines of the 5*f*–5*f* transitions, whereas attempts to calculate spectral intensities are rare.

On the other hand, for XAS at the 3*d* threshold of actinides it is relatively straightforward to calculate both energy levels and spectral intensities due to dipole selection rules. The effects of the hybridization of the valence states of actinides with ligand states in compounds and the charge transfer between ligand and actinide sites are expected to result in the appearance of charge-transfer satellites in the XAS spectra. The interpretation of such satellites can provide information on the degree of the 5*f* hybridization, covalency of the compound, and the nature of the ground state.

An advanced technique, high-energy resolution fluorescence-detection X-ray absorption spectroscopy (HERFD-XAS), has been recently used for measurements at the 3*d* edge of U compounds (14, 15). This has led to a tremendous improvement in the experimental resolution and revealed additional structures in the XAS spectra, not measurable before. We demonstrate, using ThO_2, that the HERFD-XAS technique now allows us to directly probe the CEF splittings in the 5*f* shell with the results clearly shown in the spectra. An analysis of the newly resolved charge-transfer satellites indicates significant occupancy of Th valence states, which contradicts the common view of ThO_2 as an ionic system.

Materials and Methods

The measurements at the Th 3*d* edge were performed at beamline ID26 (16) of the European Synchrotron Radiation Facility in Grenoble, France. The XAS data were measured in the HERFD mode, using an X-ray emission spectrometer (17). The HERFD spectrum of ThO_2 at the Th M_4 ($3d_{3/2} \rightarrow 5f_{5/2}, 7p$ transitions) edge was obtained by recording the outgoing photons with an energy of ~3,145.7 eV as a function of the incident energy. This emission energy corresponds to the maximum of the Th $M\beta$ ($4f_{5/2} \rightarrow 3d_{3/2}$ transitions) line. The directions of the incident and emitted photons were 45° to the surface of the sample. A total energy resolution of 0.4 eV was determined by measuring the FWHM of the elastic peak. The sample of reference bulk ThO_2 as characterized and used in refs. 18 and 19 was used for these experiments.

Significance

This work is to our knowledge the first illustration of the ability of the high-energy resolution fluorescence-detection X-ray absorption spectroscopy (HERFD-XAS) technique to directly probe the crystal-field splitting in the 5*f* shell of actinides. This is a breakthrough for actinide science, allowing for the easy extraction of desired information from the spectroscopic method, which is easy to interpret and to calculate. Furthermore, the HERFD-XAS technique allows us to resolve the charge-transfer satellites in actinide spectra that were hidden before, thus enhancing the sensitivity to the covalent character of the chemical bonding. Using ThO_2 as an example, we show that other common techniques underestimate the crystal-field strength and that ThO_2 is not an anionic compound as previously believed.

Author contributions: S.M.B., K.O.K., D.M., and D.K.S. designed research; S.M.B., K.O.K., J.R.V., D.M., and D.K.S. performed research; D.M. and D.K.S. contributed new reagents/analytic tools; S.M.B. and K.O.K. analyzed data; and S.M.B. and D.K.S. wrote the paper.

The authors declare no conflict of interest.

This article is a PNAS Direct Submission.

[1]To whom correspondence should be addressed. Email: sergei.butorin@physics.uu.se.

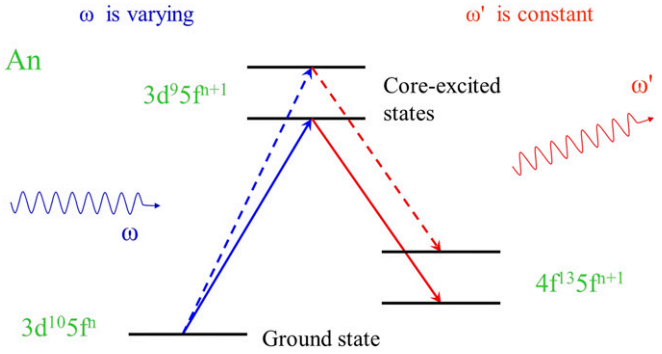

Fig. 1. Schematic representation of HERFD process for actinides (An), using 3*d*-to-4*f* transitions.

Experiments at the Ce $M_{4,5}$ edges ($3d \rightarrow 4f$, $6p$ transitions) of CeO_2 were performed at beamline 7.0.1 of the Advanced Light Source, Lawrence Berkeley National Laboratory (20). The data were measured in the total electron yield (TEY) mode, using drain current from the sample. The incidence angle of the incoming photons was close to 90° with respect to the surface of the samples. The monochromator resolution was set to ~500 meV at 890 eV. The CeO_2 sample was a pressed pellet from powder acquired from Alfa-Aesar.

The calculations were performed in framework of the Anderson impurity model (21) (AIM) in a manner described in refs. 22 and 23. Besides the inclusion of the full multiplet due to actinide intraatomic interactions, the CEF acting on the 5*f* shell (24) was taken into account.

To simulate a spectrum obtained in the HERFD-XAS mode, the resonant inelastic X-ray scattering (RIXS) map around the actinide $M\beta$ line was calculated using the Kramers–Heisenberg formula

$$I_{q_2,q_1}(\omega,\omega') = \sum_j \left| \sum_m \frac{\langle j|rC^{(1)}_{q_2}|m\rangle\langle m|rC^{(1)}_{q_1}|g\rangle}{E_g+\omega-E_m-i\Gamma_m/2} \right|^2 \times \frac{\Gamma_j/\pi}{(E_j+\omega'-E_g-\omega)^2+\Gamma_j^2}, \quad [1]$$

where $|g\rangle$, $|m\rangle$, and $|j\rangle$ are the ground, intermediate, and final states of the spectroscopic process with energies E_g, E_m, and E_j, respectively. ω and ω' are the energies of the incident and scattered/emitted photons with polarizations q_1 and q_2, respectively, and Γ_m and Γ_j are the lifetime broadenings of the intermediate and final states in terms of half width at half maximum (HWHM). Operators for optical dipole transitions (D) are expressed in terms of spherical tensor operators $C^{(1)}_q$. The HERFD-XAS spectrum is represented by a linear cut of such a RIXS map (14) along the diagonal of the plane defined by the incident energy axis and energy transfer axis or parallel to the incident energy axis at a constant emitted energy (the energy of the line maximum in this case) in the plane of the emitted vs. incident energies. The required Slater integrals F^k, G^k, and R^k (25); spin-orbit coupling constants ζ; and matrix elements were obtained with the modified TT-MULTIPLETS package (26–28).

Results and Discussion

The main reason for the improved resolution of the HERFD-XAS spectrum is a reduced core-hole lifetime broadening. For example, in HERFD-XAS measurements at U $M_{4,5}$ edges, the 3*d* core hole is replaced by the 4*f* core hole in the final state of the spectroscopic process (Fig. 1). This results in approximately four times better resolution because the 4*f* core-hole lifetime broadening (FWHM) is estimated to be ~0.8 eV (29) vs. ~3.2 eV for the 3*d* core hole.

A schematic representation of the HERFD spectroscopic process involving the $3d \rightarrow 5f$ electronic excitations with the consequent $4f \rightarrow 3d$ deexcitations at the actinide (An) atom is shown in Fig. 1, using a many-body approach. A couple of arbitrary transitions between the ground state of the system described by the $3d^{10}5f^n$ electronic configuration and core-excited states of the $3d^9 5f^{n+1}$ configuration for varying incident photon energy ω are depicted. The core-excited states decay to the states of the $4f^{13}5f^{n+1}$ configurations with the emittance of a photon and only photons with an energy equal to ω' are detected.

Fig. 2*A* displays the RIXS map around the $M\beta$ line of the Th(IV) ion in the cubic (eightfold ligand coordination) CEF environment calculated with Eq. **1** for the route $3d^{10}5f^0 \rightarrow 3d^9 5f^1 \rightarrow 4f^{13}5f^1$ with Γ_m and Γ_j set to 1.65 eV and 0.3 eV, respectively. The experimental X-ray polarization geometry was taken into account in calculations. Fig. 2*B* shows the calculated conventional XAS and HERFD-XAS spectra at the Th(IV) M_4 edge. The conventional XAS spectrum is represented by the transitions between the $3d^{10}5f^0$ (ground state) and $3d^9 5f^1$ (excited state) configurations. The HERFD-XAS spectrum is represented by the corresponding cut in the RIXS map. The result of the cut is a one-dimensional spectrum of intensity vs. incident energy ω obtained for fixed ω' corresponding to the main maximum of the $4f_{5/2} \rightarrow 3d_{3/2}$ line. In both cases, the Hartree–Fock values of the Slater integrals were scaled down to 80% (the reasoning is in ref. 30) and Wybourne's CEF parameters (24) for the 5*f* shell were set to $B^4_0 = -1.3$ eV and $B^6_0 = 0.55$ eV. Although the effects of the hybridization of Th states with ligand states (which lead to an appearance of low-intensity high-energy satellites, described below) were not taken into account, we can conclude that the conventional XAS and HERFD-XAS spectra agree with each other quite well. To simplify the computational framework, we compare the experimental HERFD-XAS data to calculations from conventional XAS.

CeO_2 is often used by researchers in the actinide science as a model compound and nonradioactive replacement of ThO_2 (UO_2) as an approximation for the physical and chemical properties and dynamic behavior of actinide materials in particular situations. However, there are significant differences between CeO_2 and ThO_2 from the electronic structure point of view. According

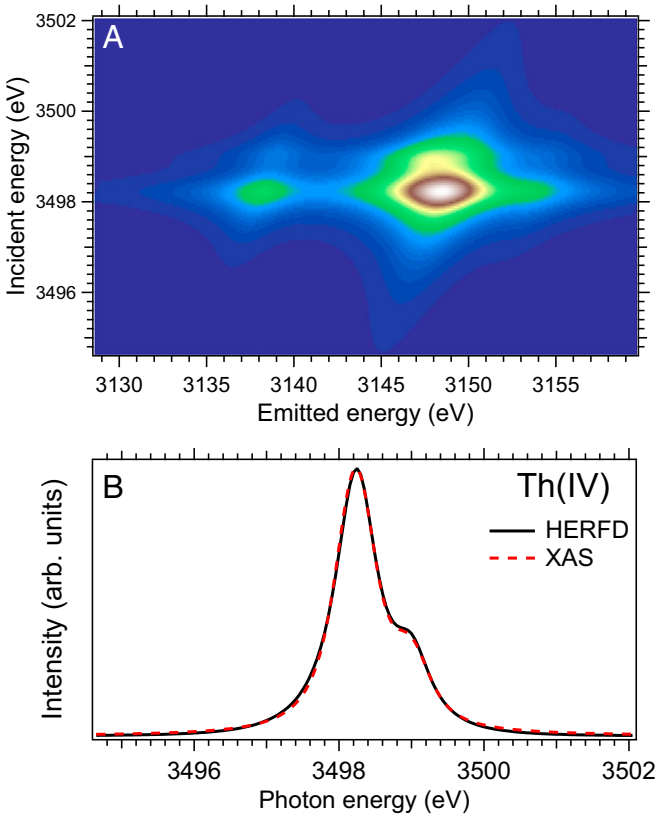

Fig. 2. Calculated RIXS map around the $M\beta$ line of the Th(IV) ion in the cubic CEF environment (*A*) and HERFD-XAS and conventional XAS spectra at the Th(IV) M_4 edge (*B*).

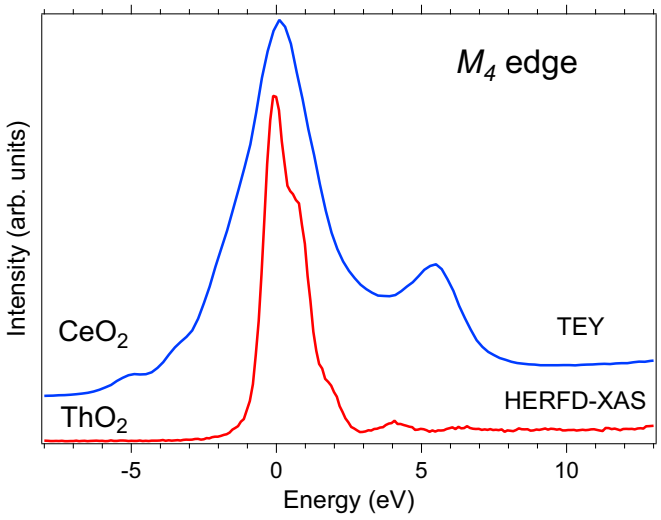

Fig. 3. XAS spectra at M_4 edge of CeO_2 and ThO_2.

to the local-density approximation with added Coulomb U interaction (LDA + U) calculations (31), the top of the valence band consists mainly of the O 2p and Ce 5d states whereas the bottom of the conduction band is dominated by Ce 4f states. In ThO_2, however, the unoccupied Th 5f states lie higher in energy so that the main weight at the bottom of the conduction band is formed by the Th 6d states. CeO_2 is considered a highly covalent compound and ThO_2 is not.

The spectra recorded at the M_4 edge of ThO_2 and CeO_2 also reveal some differences as shown in Fig. 3. Because the M_4 edge of ThO_2 is represented by the $3d \rightarrow 5f$ transitions and the M_4 edge of CeO_2 is represented by the $3d \rightarrow 4f$ transitions, the spectra were brought onto the same energy scale by setting the energy of the main maximum to 0 eV. The CeO_2 spectrum exhibits a distinct and strong high-energy satellite at ~5.5 eV above the main line whereas only weak high-energy structures at around 2.2 eV, 4.2 eV, and 6.4 eV above the main maximum are found in ThO_2. In addition, the main line of the ThO_2 spectrum has a shoulder at ~0.8 eV. The high-energy satellite in the CeO_2 spectrum has been discussed before (22, 32) and shown to arise from Ce 4f – O 2p charge transfer as a result of strong Ce 4f – O 2p hybridization and significant $4f^0$ and $4f^1\underline{v}^1$ configurational mixing in the ground state, where $\underline{v}$ stands for an electronic hole in the O 2p band. The XAS spectrum at the Ce $M_{4,5}$ edges of CeO_2 was well reproduced by the AIM calculations for the Ce(IV) system. The CeO_2 spectrum appears significantly broader than that of ThO_2 because of a wider multiplet spread of the $3d^9 4f^2\underline{v}^1$ configuration caused by the stronger 3d–4f interaction compared with the 3d(4f)–5f interaction in ThO_2 (figure 5 in ref. 32). The 4f occupancy in the ground state was found to be about 0.5 electrons, which confirms the highly covalent character of CeO_2.

For ThO_2, if the values for the AIM parameters previously used (33) to calculate the Th 4f X-ray photoemission (XPS) spectrum are adopted for calculations of the XAS spectrum at the Th(IV) M_4 edge, it is difficult to reproduce the high-energy (charge-transfer) satellites. This is because the emphasis in the XPS calculations was on the Th 5f – O 2p hybridization and charge transfer so that the ground state of the system was described as a mixture of the $5f^0$ and $5f^1\underline{v}^1$ configurations (see also ref. 34). However, the Th 6d – O 2p charge transfer might be more energetically favorable because the Th 6d states are dominant at the bottom of the conduction band of ThO_2. The charge-transfer energy is expected to be lower so that it is easier for an electron to hop from the O 2p band into unoccupied Th 6d states and the ground state of the system can be expressed as a mixture of the $5f^0$, $5f^0 6d^1\underline{v}^1$, and $5f^1\underline{v}^1$ configurations.

Fig. 4 shows that the latter approach allows one to obtain the high-energy structures in the calculated XAS spectrum at the Th M_4 edge. In particular, the structure at around 3,492.5 eV appears in the calculated spectrum upon inclusion of the Th 6d – O 2p charge transfer via Th 6d – Th 5f – O 2p hybridization. The multiplet poles of the calculated transitions can also be found at energies around 3,490.5 and 3,493.7 eV, although their intensities are lower in comparison with the corresponding structures in the measured spectrum. Note that the dashed curve in Fig. 4 is a HERFD-XAS spectrum corrected for self-absorption effects by using the algorithm implemented in the "XANES dactyloscope" program (https://www.cells.es/en/beamlines/bl22-claess/software). We point out that self-absorption correction algorithms used by the XAS community do introduce some uncertainty for the absorption edges with sharp and strong lines and low postedge background contribution, such as $L_{2,3}$ edges of transition elements and $M_{4,5}$ edges of rare earths and actinides.

In our AIM calculations for the Th(IV) system, the ground (final) state for the XAS process was described as a combination

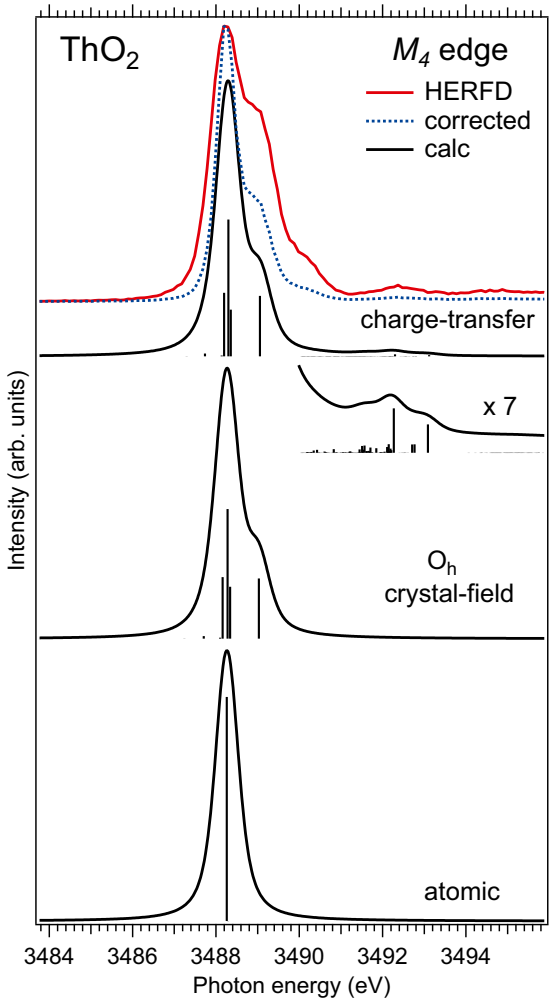

Fig. 4. Experimental and calculated XAS spectra at the Th M_4 edge of ThO_2. The spectra are calculated using atomic and CEF multiplet theory for the Th(IV) ion and the Anderson impurity model, respectively. The dashed curve represents the HERFD-XAS spectrum corrected for self-absorption effects (https://www.cells.es/en/beamlines/bl22-claess/software) and normalized to the maximum of the as-measured spectrum.

of the $5f^0$, $5f^0 6d^1\underline{v}^1$, and $5f^1\underline{v}^1$ ($3d^9 5f^1$, $3d^9 5f^1 6d^1\underline{v}^1$, and $3d^9 5f^2\underline{v}^1$) configurations. The model parameters had the following values: $U_{ff} = 4.0$ eV, $U_{fc} = 6.0$ eV, $U_{dc} - U_{df} = 2.0$ eV, $V_g = 1.1$ eV, and $V_m = 0.7$ eV, where U_{ff} (U_{df}) and U_{fc} (U_{dc}) are the $5f - 5f$ ($6d - 5f$) Coulomb interaction and core-hole potential acting on the $5f$ ($6d$) electron, respectively, and V_g and V_m are hybridization terms in the ground and final states. V_m was set smaller to take into account the configuration dependence (35) of V. Whereas in the LDA + U calculations (31, 36) for ThO_2 somewhat larger values of U_{ff} were applied (5 eV and 6 eV, respectively), $U_{ff} \simeq 4.0$ eV was deduced from the fit of the Th $4f$ XPS data (33). In addition, according to estimations in ref. 37, U_{df} can be as large as $U_{df} \simeq U_{fc}/2$.

In the limit of $V \to 0$, the difference between the configuration averaged energies for the ground state was $E(5f^0 6d^1\underline{v}^1) - E(5f^0) = \epsilon_{6d} - \epsilon_n = 5.0$ eV and $E(5f^1\underline{v}^1) - E(5f^0) = \epsilon_f - \epsilon_n = 8.0$ eV and for the final state it was $E(3d^9 5f^1 6d^1\underline{v}^1) - E(3d^9 5f^1) = \epsilon_{6d} - \epsilon_n + U_{df} - U_{dc} = 3.0$ eV and $E(3d^9 5f^2\underline{v}^1) - E(3d^9 5f^1) = \epsilon_f - \epsilon_n + U_{ff} - U_{fc} = 6.0$ eV, where ϵ_f, ϵ_{6d}, and ϵ_n are one-electron energies of Th $5f$, $6d$, and O $2p$ levels. The Slater integrals were scaled down to 80% of their Hartree–Fock values. The CEF parameters for the Th $5f$ shell were set to $B_0^4 = -1.30$ eV and $B_0^6 = 0.55$ eV and for the Th $6d$ shell to $10Dq = -3.5$ eV (38). Γ_m was set to 0.3 eV and an additional Gaussian broadening was applied to match the experimental resolution.

These calculations gave the contributions of the $5f^0 6d^1\underline{v}^1$ and $5f^1\underline{v}^1$ in the ground state of ThO_2 to be 20% and 11%, respectively; i.e., the occupancy of the Th $6d$ states (0.20 electrons) is larger than that of the Th $5f$ states (0.11 electrons). This result does not support the ionic character of ThO_2 and is also in agreement with the LDA + U (36) and hybrid-density functional (39) calculations that show the occupied Th $6d$ density of states (DOS) in the valence band of ThO_2 to be about two times higher than the occupied Th $5f$ DOS.

The improved resolution of the HERFD-XAS technique allows us to resolve the shoulder at ∼0.8 eV above the main maximum of the Th M_4 edge of ThO_2 (conventional XAS spectra in refs. 4 and 40). The origin of this shoulder becomes clear from a comparison of the experimental data with atomic and CEF multiplet theory for the Th(IV) ion in Fig. 4. The atomic multiplet calculations for the transitions between the $3d^{10}5f^0$ and $3d^9 5f^1$ configuration in the $^1S_0$ ground state produce a single multiplet pole whereas putting the Th(IV) ion in the cubic (O_h) CEF environment reveals CEF split states of the $3d^9 5f^1$ configuration, thus producing the shoulder at ∼0.8 eV above the main peak in the calculated spectrum for the CEF parameter values of $B_0^4 = -1.30$ eV and $B_0^6 = 0.55$ eV. The improvement in resolution offered by HERFD-XAS now allows probing the CEF interactions for the $5f$ shell and extracting the information about the CEF effects directly from the XAS data in the manner commonly used for the $L_{2,3}$ edges of $3d$ transition metal systems.

Specifically for ThO_2, it is difficult to accurately determine the CEF strength with other techniques. For commonly used methods, such as optical and EPR spectroscopies, the ThO_2 sample is usually doped with a small concentration of another actinide ion into the ThO_2 lattice to observe the $5f - 5f$ excitation pattern in the spectra. However, this may cause a local lattice distortion around the doped actinide ion, thus generating larger uncertainties in quantities derived from the fit of the spectra. For example, our determined values for CEF parameters B_0^4 and B_0^6 are somewhat larger than those obtained for Am-doped (41) and Cm-doped (42) ThO_2.

Improved energy resolution demonstrates the shape sensitivity of the actinide M_4 edge to the strength of the crystal-field interaction and to the degree of covalency in the chemical bonding. Therefore, as in case of the $L_{2,3}$ edges of $3d$ transition metal systems, detailed analysis of the $M_{4,5}$ edges spectral shapes of actinide compounds with the partially filled $5f$ shell enables characterization of the ground state and low-lying excited states that define physical properties of these compounds (for example, analysis of the results of the temperature-dependent measurements or measurements in varying X-ray polarization geometries).

ACKNOWLEDGMENTS. We thank Dr. D. Hudry for providing the ThO_2 sample. This research was supported by the Director, Office of Science, Office of Basic Energy Sciences, Division of Chemical Sciences, Geosciences, and Biosciences Heavy Element Chemistry program (D.K.S.) and the Advanced Light Source is supported by the Director, Office of Science, Basic Energy Sciences; both supported by the US Department of Energy at Lawrence Berkeley National Laboratory under Contract DE-AC02-05CH11231.

1. de Groot FMF (1994) X-ray absorption and dichroism of transition metals and their compounds. *J Electron Spectrosc Relat Phenom* 67(4):529–622.
2. Raboud P-A, Dousse J-Cl, Hoszowska J, Savoy I (2000) L_1 to N_5 atomic level widths of thorium and uranium as inferred from measurements of *L* and *M* x-ray spectra. *Phys Rev A* 61(1):012507.
3. Petiau J, et al. (1986) Delocalized versus localized unoccupied 5f states and the uranium site structure in uranium oxides and glasses probed by x-ray-absorption near-edge structure. *Phys Rev B Condens Matter* 34(10):7350–7361.
4. Kalkowski G, Kaindl G, Brewer WD, Krone W (1987) Near-edge x-ray-absorption fine structure in uranium compounds. *Phys Rev B Condens Matter* 35(6):2667–2677.
5. Butorin SM (2000) Resonant inelastic X-ray scattering as a probe of optical scale excitations in strongly electron-correlated systems: Quasi-localized view. *J Electron Spectrosc Relat Phenom* 110–111:213–233.
6. Nilsson HJ, Tyliszczak T, Wilson RE, Werme L, Shuh DK (2005) Soft X-ray scanning transmission X-ray microscopy (STXM) of actinide particles. *Anal Bioanal Chem* 383(1):41–47.
7. Moore KT, van der Laan G, Haire RG, Wall MA, Schwartz AJ (2006) Oxidation and aging in U and Pu probed by spin-orbit sum rule analysis: Indications for covalent metal-oxide bonds. *Phys Rev B* 73(3):033109.
8. Tobin JG, Yu S-W (2011) Orbital specificity in the unoccupied states of UO_2 from resonant inverse photoelectron spectroscopy. *Phys Rev Lett* 107(16):167406.
9. Liu G, Beitz JV (2010) Optical spectra and electronic structure. *Chemistry of the Actinide and Transactinide Elements*, eds Morss LR, Edelstein N, Fuger J (Springer, Dordrecht, The Netherlands), pp 2013–2111.
10. Amoretti G, et al. (1986) Actinide and rare earth ions in single crystals of ThO_2: Preparation, EPR studies and related problems. *J Less Common Met* 122:35–45.
11. Seaman LA, et al. (2012) Probing the 5f orbital contribution to the bonding in a U(V) ketimide complex. *J Am Chem Soc* 134(10):4931–4940.
12. Amoretti G, et al. (1989) 5f-electron states in uranium dioxide investigated using high-resolution neutron spectroscopy. *Phys Rev B Condens Matter* 40(3):1856–1870.
13. Nakotte H, et al. (2010) Crystal fields in UO_2 - Revisited. *J Phys Conf Ser* 251(1):012002.
14. Kvashnina KO, Butorin SM, Martin P, Glatzel P (2013) Chemical state of complex uranium oxides. *Phys Rev Lett* 111(25):253002.
15. Kvashnina KO, Kvashnin YO, Butorin SM (2014) Role of resonant inelastic X-ray scattering in high-resolution core-level spectroscopy of actinide materials. *J Electron Spectrosc Relat Phenom* 194:27–36.
16. Gauthier C, Solé VA, Signorato R, Goulon J, Moguiline E (1999) The ESRF beamline ID26: X-ray absorption on ultra dilute sample. *J Synchrotron Radiat* 6(Pt 3): 164–166.
17. Glatzel P, Bergmann U (2005) High resolution 1s core hole X-ray spectroscopy in 3d transition metal complexes: Electronic and structural information. *Coord Chem Rev* 249(1–2):65–95.
18. Hudry D, et al. (2014) Thorium/uranium mixed oxide nanocrystals: Synthesis, structural characterization and magnetic properties. *Nano Res* 7(1):119–131.
19. Hudry D, et al. (2012) Non-aqueous synthesis of isotropic and anisotropic actinide oxide nanocrystals. *Chemistry* 18(27):8283–8287.
20. Warwick T, Heimann P, Mossessian D, McKinney W, Padmore H (1995) Performance of a high resolution, high flux density SGM undulator beamline at the ALS. *Rev Sci Instrum* 66(2):2037–2040.
21. Anderson PW (1961) Localized magnetic states in metals. *Phys Rev B* 124(1):41–53.
22. Butorin SM, et al. (1996) Resonant X-ray fluorescence spectroscopy of correlated systems: A probe of charge-transfer excitations. *Phys Rev Lett* 77(3):574–577.
23. Nakazawa M, Ogasawara H, Kotani A (2002) Theory of polarization dependence in resonant X-ray emission spectra of a uranium compound. *Surf Rev Lett* 9(2): 1149–1153.
24. Wybourne BG (1963) *Spectroscopic Properties of Rare Earths* (Wiley, New York).
25. Slater JC (1929) The theory of complex spectra. *Phys Rev* 34(10):1293–1322.
26. Cowan RD (1981) *Theory of Atomic Structure and Spectra* (Univ of California Press, Berkeley).
27. Butler PH (1981) *Point Group Symmetry Applications: Methods and Tables* (Plenum, New York).
28. Thole BT, van der Laan G, Butler PH (1988) Spin-mixed ground state of Fe phthalocyanine and the temperature-dependent branching ratio in X-ray absorption spectroscopy. *Chem Phys Lett* 149(3):295–299.
29. Fuggle JC, Alvarado SF (1980) Core-level lifetimes as determined by x-ray photoelectron spectroscopy measurements. *Phys Rev A* 22(4):1615–1624.

30. Sugar J (1972) Potential-barrier effects in photoabsorption. II. Interpretation of photoabsorption resonances in lanthanide metals at the 4*d*-electron threshold. *Phys Rev B* 5(5): 1785–1792.
31. Sevik C, Çağin T (2009) Mechanical and electronic properties of CeO_2, ThO_2, and $(Ce,Th)O_2$ alloys. *Phys Rev B* 80(1):014108.
32. Ogasawara H, Kotani A, Okada K, Thole BT (1991) Theory of x-ray absorption spectra in PrO_2 and some other rare-earth compounds. *Phys Rev B* 43(1):854–859.
33. Kotani A, Ogasawara H (1993) Theory of core-level spectroscopy in actinide systems. *Physica B* 186–188:16–20.
34. Gunnarsson O, Sarma DD, Hillebrecht FU, Schönhammer K (1988) Electronic structure of the light actinide oxides from electron spectroscopy. *J Appl Phys* 63(8):3676–3679.
35. Gunnarsson O, Jepsen O (1988) Configuration dependence of hopping matrix elements in the Anderson model. *Phys Rev B Condens Matter* 38(5):3568–3571.
36. Szpunar B, Szpunar JA (2013) Application of density functional theory in assessing properties of thoria and recycled fuels. *J Nucl Mater* 439(1-3):243–250.
37. Kotani A, Jo T, Parlebas JC (1988) Many-body effects in core-level spectroscopy of rare-earth compounds. *Adv Phys* 37(1):37–85.
38. Kvashnina KO, et al. (2015) Sensitivity to actinide doping of uranium compounds by resonant inelastic X-ray scattering at uranium L_3 edge. *Anal Chem* 87(17):8772–8780.
39. Wen X-D, et al. (2012) Effect of spin-orbit coupling on the actinide dioxides AnO_2 (An=Th, Pa, U, Np, Pu, and Am): A screened hybrid density functional study. *J Chem Phys* 137(15):154707.
40. Kelly TD, et al. (2014) The unoccupied electronic structure characterization of hydrothermally grown ThO2 single crystals. *Phys Stat Sol RRL* 8(3):283–286.
41. Hubert S, Thouvenot P, Edelstein N (1993) Spectroscopic studies and crystal-field analyses of Am3+ and Eu3+ in the cubic-symmetry site of ThO_2. *Phys Rev B* 48(9): 5751–5760.
42. Thouvenot P, Hubert S, Edelstein N (1994) Spectroscopic study and crystal-field analysis of Cm^{3+} in the cubic-symmetry site of ThO_2. *Phys Rev B* 50(14):9715–9720.